Progress In Electromagnetics Research Letters, Vol. 104, 161–168, 2022

A Triple Band Artificial Magnetic Conductor: Design & Analytical Model

Amina Fattouche[1, *], Lila Mouffok[1], Sami Hebib[2], and Ali Mansoul[3]

Abstract—A triple band Artificial Magnetic Conductor (AMC) featuring zero reflection phase at 1.18 GHz, 1.59 GHz, and 2.45 GHz is designed and modeled. The two lower frequencies are intended for GNSS while the upper one is for ISM applications. The AMC's unit cell printed on a dielectric substrate with a permittivity of 10.2 exhibits a compact dimension of $25 \times 25\,\text{mm}^2$ ($0.09\lambda c \times 0.09\lambda c$, λc: the free space wavelength at 1.18 GHz). A square patch is designed to achieve the first resonance (1.18 GHz) while the other two resonance frequencies (1.59 GHz and 2.45 GHz) are generated by etching two square slots in this square patch. All the three resonant frequencies are consequently adjusted quasi-independently of each other. In addition, an analytical model based on the LC formulation is developed and validated by electromagnetic simulation. It allows fast prediction of the three frequencies at which the meta-material reflects incident waves in-phase. Finally, the accuracy of the proposed model is studied, showing a good agreement between electromagnetic simulation and analytical results with an estimation error lower than 120 MHz.

1. INTRODUCTION

Metamaterials have a great potential in antenna applications. They can present different behaviors, such as Electromagnetic Band-Gap (EBG) properties and Artificial Magnetic Conductor (AMC) properties [1]. They became very popular in the microwave and antenna community thanks to their compact size and applications derived from their interesting characteristics of surface wave suppression and in-phase reflection coefficient properties [2–4]. AMC structures are periodic structures usually used as a ground plane for low-profile conformal antennas. They are characterized by frequencies where the reflection coefficient phase is zero degrees. This property improves antenna directivity.

Diverse AMC structures have been developed, at broad frequency band [5, 6], single frequency band [7–9], and dual frequency band [10–13]. However, to our knowledge, few designs are reported for triple frequency band AMC [14–17]. In [14], a unit cell AMC of $0.34\lambda c \times 0.34\lambda c$ (λc: effective wavelength at 2.3 GHz) is designed for three operating frequencies: 2.3 GHz, 5.8 GHz, and 8.36 GHz. In [15], a miniaturized tri-band AMC unit cell with a total dimension of $0.2\lambda c \times 0.2\lambda c$ (λc at 2.3 GHz) is presented. It shows a zero-reflection phase at 2.3 GHz, 4 GHz, and 5.55 GHz. Besides having their three operating frequencies quite interrelated, the previous triple band AMCs [14, 15] are given without an analytical model. In [16], a triple band AMC with its analytical model is proposed. The unit cell has a dimension of $0.37\lambda c \times 0.37\lambda c$ (λc at 3.6 GHz), and it shows zero reflection phase at 3.6 GHz, 5.86 GHz, and 8.53 GHz. The analytical model exhibits a frequency shift of 250 MHz compared to electromagnetic simulation. Another design of a triple band AMC with its analytical model is introduced in [17]. The dimensions of its unit cell are $0.38\lambda c \times 0.38\lambda c$ (λc at 3.36 GHz). A resonant frequency difference up to

Received 8 March 2022, Accepted 6 June 2022, Scheduled 20 June 2022

* Corresponding author: Amina Fattouche (amina.fattouche@univ-blida.dz).

[1] Aeronautical Sciences Laboratory, Institute of Aeronautics and Spatial Studies, University of Blida 1, Algeria. [2] DIC Laboratory, Faculty of Technology, University of Blida 1, Algeria. [3] Division Telecom, Centre de Développement des Technologies Avancées (CDTA), Algiers, Algeria.

280 MHz is obtained through analysis and electromagnetic simulation. The gain of the antenna placed above this AMC is enhanced at the resonance frequencies 3.36 GHz, 5.96 GHz, and 9.09 GHz.

In this paper, a simple design of a triple band AMC is proposed. Moreover, an analytical model is also developed to predict its three operating frequency resonances with a shift lower than 120 MHz compared to electromagnetic simulation. The originality of the proposed structure is that the three operating frequencies are quasi-independent and easily estimated analytically.

2. PROPOSED TRI-BAND AMC

2.1. Triple Band AMC Design

The proposed triple band AMC cell is shown in Fig. 1(a). It consists of a square patch with a dimension of $w_1 = 22.4$ mm, printed on a substrate with $W_{amc} = 25$ mm, thickness of $h = 5$ mm, and permittivity of 10.2. This square patch is responsible for operation at 1.18 GHz. Two square slots with a width of $b = 0.4$ mm are inserted in order to obtain the middle and highest operating frequencies. The bigger one (colored in blue) with a dimension of $w_2 = 20.95$ mm allows operation at 1.59 GHz while the smaller one (colored in red) with a dimension of $w_3 = 16$ mm allows operation at 2.45 GHz. Therefore, the lowest ($f_1 = 1.18$ GHz), middle ($f_2 = 1.59$ GHz), and highest ($f_3 = 2.45$ GHz) frequencies are mainly and independently controlled by w_1, w_2, and w_3, respectively. Moreover, it is also possible to operate on more frequencies (quad-band AMC, penta-band AMC ... etc.) by etching more square slots into the metallic patch.

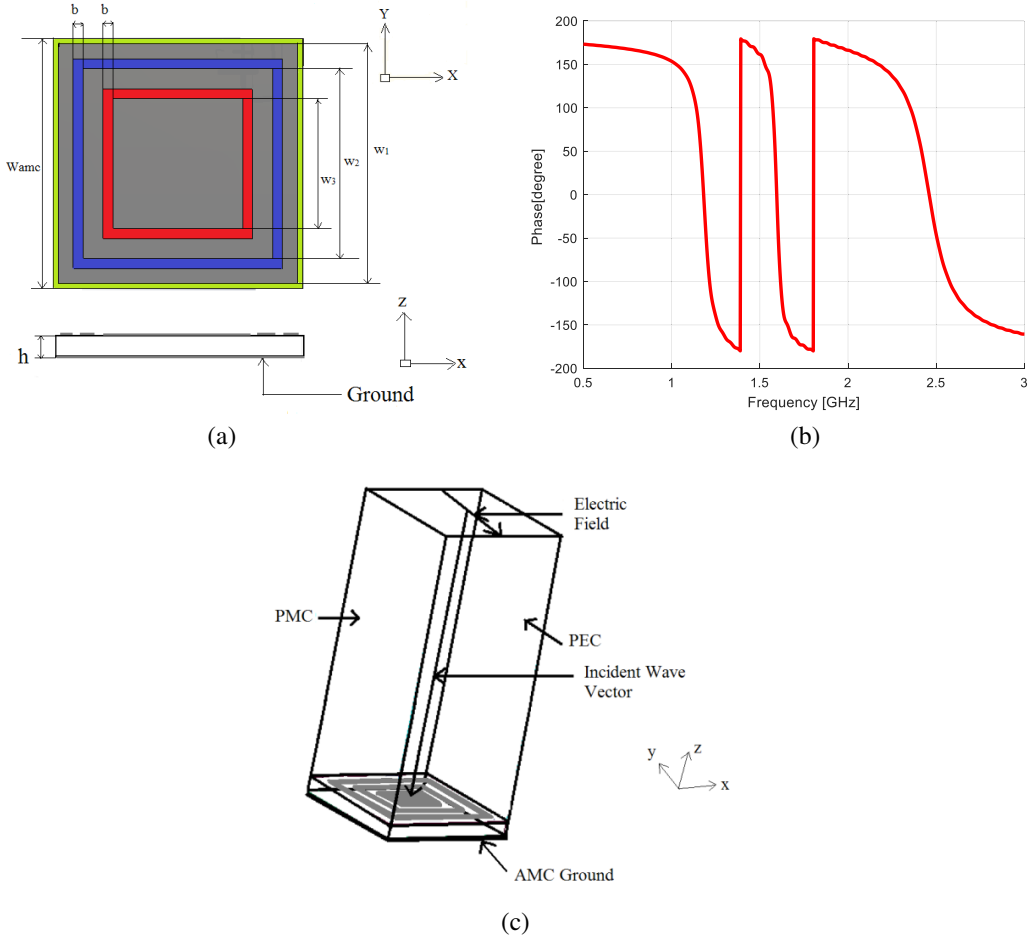

Figure 1. (a) Proposed tri-band AMC unit cell, (b) phase reflection coefficient, (c) AMC unit cell simulation setup.

The electromagnetic simulation was performed using the time domain solver of CST Microwave Studio by placing the grounded tri-band unit cell in a radiation box, as shown in Fig. 1(c). Two opposite faces of the box make a perfect electric conductor (PEC) while the remaining two opposite faces are set as a perfect magnetic conductor (PMC). These boundary conditions are used for imaging the unit cell to infinite extent in both x and y axes [18], thus giving an effect of periodic arrangement of the unit cell. Plane wave excitation is used where the electric field is parallel to x-axis, and the wave vector normally illuminates the surface of the AMC unit cell. Obtained simulation results in terms of phase reflection coefficient of the triple band AMC are plotted in Fig. 1(b). A null is observed in the reflection coefficient phase for the lowest ($f_1 = 1.18\,\text{GHz}$), middle ($f_2 = 1.59\,\text{GHz}$), and highest ($f_3 = 2.45\,\text{GHz}$) frequencies.

2.2. Analytical Model

To analytically analyze AMC structures, various methods have been investigated. One of them consists in the use of LC formulation that is derived from conformal mapping theory [19]. As a matter of fact, the three resonance frequencies can be analytically determined, by considering that the tri-band AMC structure is equivalent to an LC circuit for each frequency. The variation in the patch size and permittivity influences the capacitance C_i whereas the substrate thickness and its permeability mainly affect the inductance L_i. Therefore, the two parameters L_i and C_i can be used to control the three resonant frequencies. They can be expressed as functions of physical dimensions and dielectric substrate properties as follows [20].

$$L_i = \mu_r \left(\alpha_i h^{\beta_i}\right) \tag{1}$$

$$C_i = \left(\frac{\delta i w_i}{\pi}\right)(\varepsilon_0 + \varepsilon_r)\cosh^{-1}\left(\frac{0.0034 W_{amc^3} - 0.92 W_{amc^2} + W_{amc}}{g_i}\right) \tag{2}$$

$$g_i = \frac{(W_{amc} - w_i)}{2} \tag{3}$$

$$f_i = \frac{1}{2\pi\sqrt{L_i C_i}} \tag{4}$$

where μ_r, ε_0, ε_r, h, w_i, and W_{amc} represent substrate permeability, vacuum permittivity, substrate relative permittivity, substrate thickness, patch width, and substrate width, respectively. Table 1 presents correction factors α_i, β_i, and δ_i which were at first obtained by electromagnetic simulation (CST Microwave studio), and then fixed for the proposed analytical model. These correction factors were determined by minimizing discrepancy between electromagnetic simulation (CST) and analytical results which were given by solving Eq. (4). It is important to underline that these correction factors are quite independent of the three operating frequencies of the AMC. Fig. 2, Fig. 3, and Fig. 4 depict the comparison of analytical results without correction [20], simulation results, and analytical results with correction for various parameters of the tri-band AMC unit cell: substrate width W_{amc}, patch width w_1, and the substrate thickness h. It is clearly seen that analytical results with correction show good agreements with the simulation ones for every varied variable (W_{amc}, w_1, and h).

Table 1. The correction factors of the proposed analytical model.

i	1	2	3
α	0.110	0.020	0.080
β	0.200	−0.150	0.126
δ	1.685	0.869	0.685

To further validate the proposed model, a comparison of its results with simulated ones is given in Table 2. It shows a good agreement between the results with a frequency estimation error (Δf) ranging between 20 MHz and 120 MHz. The dimensions of the structure are: $W_{amc} = 25\,\text{mm}$, $w_1 = 22.4\,\text{mm}$,

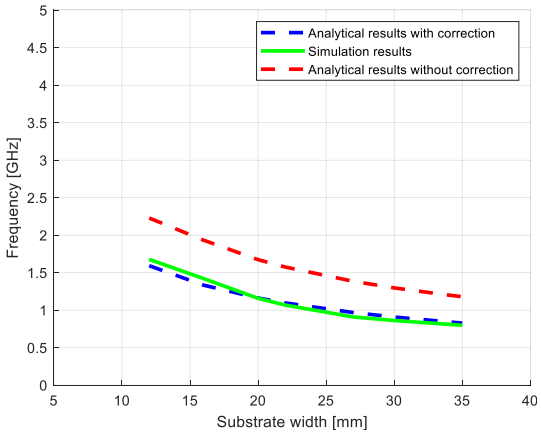

Figure 2. Analytical results with correction, simulation results, and analytical results without correction for varied substrate width W_{amc}.

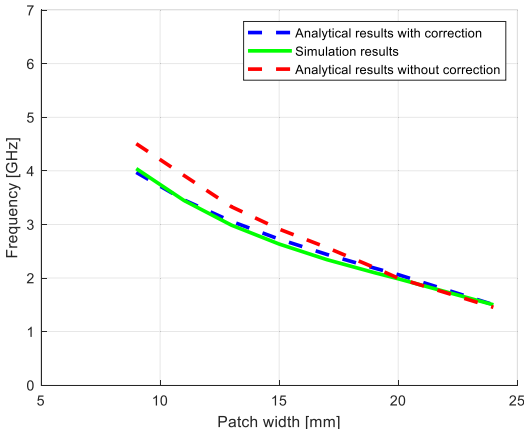

Figure 3. Analytical results with correction, simulation results, and analytical results without correction for varied patch width w_1.

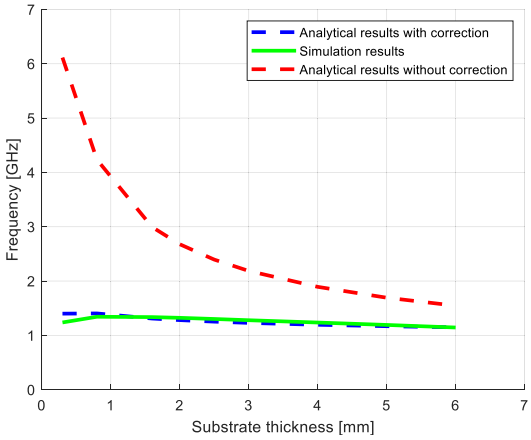

Figure 4. Analytical results with correction, simulation results, and analytical results without correction for varied substrate thickness h.

$w_2 = 20.95\,\text{mm}$, $w_3 = 16\,\text{mm}$, $b = 0.4\,\text{mm}$, $h = 5\,\text{mm}$, $\varepsilon_r = 10.2$, and $\mu_r = 1$. These dimensions were optimized to provide a simulated zero-reflection phase at 1.18 GHz, 1.59 GHz, and 2.45 GHz. It is important to highlight that the developed analytical model is easy to implement and especially less time consuming than electromagnetic simulations for the design of the previously described triband AMC. Finally, this model is also suitable for AMC operating at more than three frequency bands, by simply adding a new correction factor for each added frequency.

2.3. Parametric Study

In order to further investigate the proposed analytical model, a parametric study of its parameters is carried out and discussed. First, Fig. 5 shows the effect of the variation of w_i ($i = 1, 2$, and 3), which is the main parameter of the AMC, on the three resonant frequencies. It is observed that when the size of the AMC cell increases (while g_i is kept constant), the null phase frequency decreases. Analytical (dashed lines) and simulated (solid lines) results are in good agreement with a frequency estimation error lower than 100 MHz when w_1 ranges between 15 mm and 35 mm (green color). The second resonance f_2 (w_2 curve in blue color), which shifts from 1.4 to 2 GHz, is given with a maximum estimation error of 115 MHz. Since the values of w_2 are limited between w_1 and w_3, and the total dimension of the proposed tri-band AMC is $25 \times 25\,\text{mm}^2$, the variation range of w_2 is from 17 to 23 mm. For the highest frequency

Table 2. Comparison of results obtained from analytical modeling and simulation.

	Lowest frequency (f_1)	**Middle frequency (f_2)**	**Highest frequency (f_3)**	**Computing time (s)**
Analytical	1.16 GHz	1.66 GHz	2.57 GHz	0.1
Simulation	1.18 GHz	1.59 GHz	2.45 GHz	480
Estimation error (Δf)	20 MHz	70 MHz	120 MHz	/

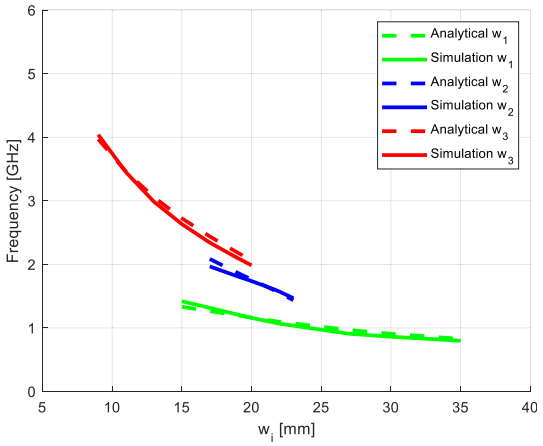

Figure 5. Impact of the patch width w_i on the resonance frequencies.

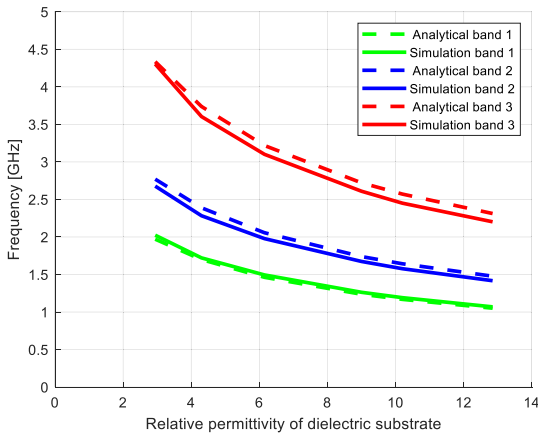

Figure 6. Impact of the substrate relative permittivity ε_r.

f_3, the max value of w_3 is limited by w_2. Therefore, the variation range of w_3 is from 9 to 20 mm. An estimation error less than 77 MHz is obtained. Fig. 6 illustrates the simulated and analytical results in terms of resonant frequencies as a function of relative permittivity. For comparison, the results for the three frequency bands are plotted together with different colors. It can be noticed that the analytical results agree well with the simulated ones, with estimation errors up to 100 MHz, 115 MHz, and 77 MHz for the lower, middle, and higher resonance frequencies, respectively.

The last parametric study deals with the effect of the substrate thickness h on the AMC's resonant frequencies. The analytical and electromagnetic simulation results of this study are plotted in Fig. 7. A good agreement can be found between these results with a maximum estimation error of 179 MHz. In addition, the substrate thickness variation (h from 0.3 to 6 mm) leads to a resonant frequency variation from 1.1 to 3.1 GHz. It can be concluded that the effect of the dielectric properties (dielectric permittivity and thickness) is correctly taken into account in the developed analytical model.

3. INDEPENDENTLY ADJUSTED TRI-BAND AMC

The proposed tri-band AMC has the advantage of adjusting its operating frequencies in a quasi-independent way. As previously mentioned, the first (f_1 = 1.18 GHz), second (f_2 = 1.59 GHz), and third (f_3 = 2.45 GHz) frequencies are mainly controlled by w_1, w_2, and w_3, respectively. As shown in Fig. 8(a), for different values of w_1 (from 20 to 24 mm), f_1 shifts from 0.9 to 1.4 GHz while f_2 and f_3 remain unaffected. In addition, when w_2 is varied from 19 to 22 mm, only f_2 shifts from 1.5 to 1.7 GHz, as illustrated in Fig. 8(b). Finally, as shown in Fig. 8(c), the variation of w_3 from 14 to 18 mm affects only the higher frequency f_3, which moves from 2.3 GHz to 2.75 GHz.

Table 3. Impact of the variation of w_i on the three resonance frequencies.

Resonant frequency shift	Variation of w_1 [20 to 24 mm]	Variation of w_2 [19 to 22 mm]	Variation of w_3 [14 to 18 mm]
Δf_1	**500 MHz**	28 MHz	10 MHz
Δf_2	20 MHz	**200 MHz**	30 MHz
Δf_3	10 MHz	16 MHz	**450 MHz**

The impact of w_i ($i = 1,\ 2$, and 3) variation on each resonant frequency is summarized in Table 3. As we can see, the three resonance frequencies are mainly controlled by w_1, w_2, and w_3, respectively. Relatively small shifts are, however, observed for the other resonant frequencies. In fact, by varying w_1 from 20 to 24 mm, a shift of 20 MHz and 10 MHz is obtained for the second and third frequencies, respectively. The variation of w_2 from 19 to 22 mm leads to a shift of 28 MHz and 16 MHz for the first and third frequencies, respectively. Finally, shifts of 10 MHz for the first frequency and 30 MHz for the second one are attained from the variation of w_3.

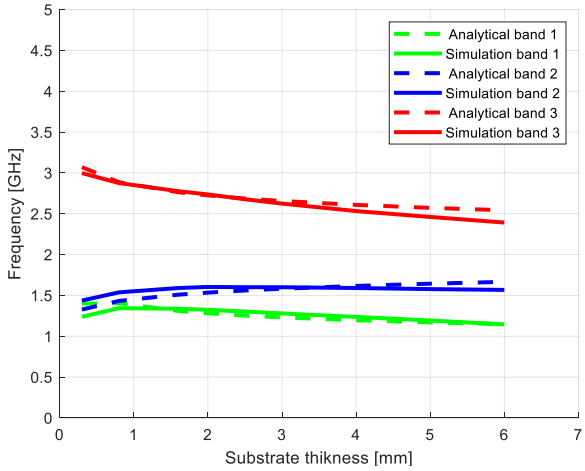

Figure 7. Impact of the substrate thickness h.

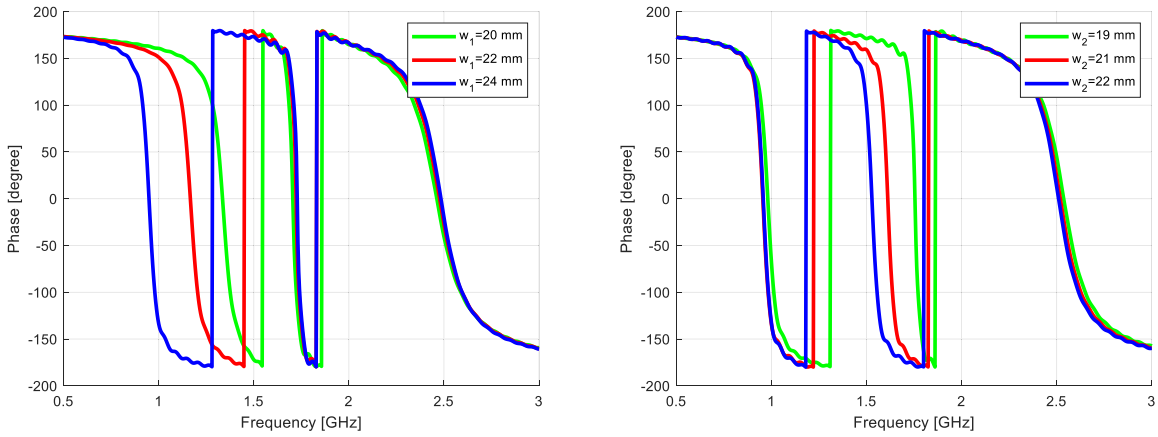

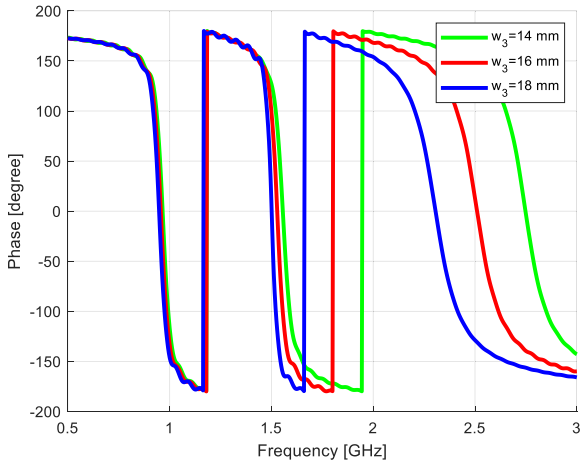

(c)

Figure 8. Simulated phase reflection coefficients: impact of the variation of (a) w_1, (b) w_2, and (c) w_3.

4. CONCLUSION

In this paper, a novel triple-band Artificial Magnetic Conductor (AMC) has been proposed and analytically modeled for GNSS applications (1.18 GHz and 1.59 GHz) and ISM applications (2.45 GHz). Its unit cell presents a total dimension of $0.09\lambda c \times 0.09\lambda c$ (λc: the free space wavelength at 1.18 GHz) when being printed on a 5 mm-thickness dielectric substrate with a permittivity of 10.2. It has been shown that the three operating frequencies at which it reflects incident waves in-phase can be quasi-independently set which largely facilitates the design process. Moreover, an analytical model based on LC formulation of the tri-band AMC is developed and validated by means of electromagnetic simulation. Besides predicting with an estimation error lower than 120 MHz the three null phase frequencies, this model allows us to save a considerable amount of time (ratio of 1280) compared to the electromagnetic simulation. Finally, the proposed AMC design could also be used with more than three operating frequencies or with frequencies very close to each other.

REFERENCES

1. Sievenpiper, P., L. Zhang, R. F. J Broas, et al., "High impedance electromagnetic surfaces with a forbidden frequency band," *IEEE Transactions on Microwave Theory and Techniques*, Vol. 47, No. 11, 2059–2074, 1999, DOI: 10.1109/22.798001.
2. Alibakhshikenari, M., et al., "Surface wave reduction in antenna arrays using metasurface inclusion for MIMO and SAR systems," *Radio Science*, Vol. 54, No. 11, 1067–1075, 2019.
3. Alibakhshikenari, M., B. S. Virdee, and E. Limiti, "Study on isolation and radiation behaviours of a 34×34 array-antennas based on SIW and metasurface properties for applications in terahertz and over 125–300 GHz," *Optik*, Vol. 206, Art. No. 163222, Mar. 2020.
4. Alibakhshikenari, M., B. S. Virdee, P. Shukla, et al., "Metamaterial-Inspired antenna array for application in Microwave breast imaging systems for tumor detection," *IEEE Access*, Vol. 8, 174667–174678, 2020.
5. Ge, Y., Y. J. Zhao, and J. Q. Chen, "Wideband RCS reduction and gain enhancement for a patch antenna with broadband AMC structure," *Radio Engineering*, Vol. 2, No. 1, 45–52, 2019.
6. Ren, Y., X. Guo, and C. Li, "Broadband circular polarized antenna loaded with AMC structure," *Progress In Electromagnetics Research Letters*, Vol. 76, 113–119, 2018.

7. Sang, X.-Y., C. Yang, T.-L. Zhang, Z.-H. Yan, and R.-N. Lian, "Broadband and gain enhanced bowtie antenna with AMC ground," *Progress In Electromagnetics Research Letter*, Vol. 61, 25–30, 2016.
8. Li, M., Q. L. Li, B. Wang, C. F. Zhou, and S. W. Cheung, "A low-profile dual-polarized dipole antenna using wideband AMC reflector," *IEEE Trans. Antennas Propagation*, Vol. 66, No. 5, 2610–2615, May 2018.
9. Volkov, A. P., V. V. Kakshin, I. Yu. Ryzhov, K. V. Kozlov, and A. Yu. Grinev, "Wideband low-profile dual-polarized antenna with AMC reflector," *Progress In Electromagnetics Research Letter*, Vol. 88, 15–20, 2020.
10. Ta, S. X. and I. Park, "Dual-band low-profile crossed asymmetric dipole antenna on dual-band AMC structure," *IEEE Antennas Wireless Propagation Lett.*, Vol. 13, 587–590, 2014.
11. Chamani, Z. and S. Jahanbakht, "Improved performance of double-T monopole antenna for 2.4/5.6 GHz dual-band WLAN operation using artificial magnetic conductors," *Progress In Electromagnetics Research M*, Vol. 61, 205–213, 2017.
12. Kumar, P. and D. Ghosh, "High-gain dual-band antenna with AMC surface for satellite communications," *Journal of Electromagnetic Waves and Applications*, Vol. 35, No. 5, 604–619, Nov. 2020.
13. Sarrazin, J., A. C. Lepage, and X. Begaud, "Dual-band artificial magnetic conductor," *Appl. Phys. A*, Vol. 109, No. 4, 1075–1080, 2012.
14. Dewan, R., S. K. A. Rahim, S. F. Ausordin, and H. U. Iddi, "Design of triple band artificial magnetic conductor," *IEEE Asia-Pacific Conference on Applied Electromagnetics*, 253–256, 2012.
15. Fneish, Z., F. Mazeh, H. Ayad, A. A. Khalil, G. Faour, M. Fadlallah, and J. Jomaah, "Design of a miniaturized dual wide band and triband artificial magnetic conductor in LTE regions," *2017 Sensors Networks Smart and Emerging Technologies (SENSET)*, 978-1-5090-6011, IEEE, 2017.
16. Ghosh, A., T. Mandal, and S. Das, "Design of triple band slot-patchantenna with improved gain using triple band artificial magnetic conductor," *Radio Engineering*, Vol. 25, No. 3, 442–448, 2016.
17. Ghosh, A., V. Kumar, G. Sen, and S. Das, "Gain enhancement of triple-band patch antenna by using triple-band artificial magnetic conductor," *IET Microwaves, Antennas & Propagation*, Vol. 12, No. 8, 1400–1406, 2018.
18. Ihsan, R. R. and A. Munir, "Utilization of artificial magnetic conductor for bandwidth enhancement of square patch antenna," *7th International Conference on Telecommunication Systems, Services and Applications*, 192–195, Bali, Indonesia, 2012, DOI: 10.1109/TSSA.2012.6366049.
19. Capolino, F., *Theory and Phenomena of Metamaterials*, Chapter 32, 32–1, Taylor & Francis, 2009.
20. Suraperwata, A. V., L. Olivia, and A. Munir, "Inductance and capacitance reformulation of square patch-based artificial magnetic conductor," *Proc. 7th International Conference on Telecommunication Systems, Services, and Applications (TSSA)*, 187–191, 2012.